







# Antarctic Polyester Hydrolases Degrade Aliphatic and Aromatic Polyesters at Moderate Temperatures

Paula Blázquez-Sánchez,<sup>a,b</sup> Felipe Engelberger,<sup>a,b</sup>  Jerónimo Cifuentes-Anticevic,<sup>c</sup> Christian Sonnendecker,<sup>d</sup> Aransa Griñén,<sup>a,b</sup> Javiera Reyes,<sup>a,b</sup>  Beatriz Díez,<sup>c,e,f</sup> Victoria Guixé,<sup>g</sup> P. Konstantin Richter,<sup>h</sup>  Wolfgang Zimmermann,<sup>d</sup>  César A. Ramírez-Sarmiento<sup>a,b</sup>

<sup>a</sup>Institute for Biological and Medical Engineering, Schools of Engineering, Medicine and Biological Sciences, Pontificia Universidad Católica de Chile, Santiago, Chile

<sup>b</sup>ANID—Millennium Science Initiative Program—Millennium Institute for Integrative Biology (iBio), Santiago, Chile

<sup>c</sup>Department of Molecular Genetics and Microbiology, School of Biological Sciences, Pontificia Universidad Católica de Chile, Santiago, Chile

<sup>d</sup>Institute of Analytical Chemistry, Leipzig University, Leipzig, Germany

<sup>e</sup>Center for Climate and Resilience Research (CR)<sup>2</sup>, Santiago, Chile

<sup>f</sup>FONDAP Center for Genome Regulation (CGR), Santiago, Chile

<sup>g</sup>Departamento de Biología, Facultad de Ciencias, Universidad de Chile, Santiago, Chile

<sup>h</sup>Institute of Bioanalytical Chemistry, Center for Biotechnology and Biomedicine, Leipzig University, Leipzig, Germany

**ABSTRACT** Polyethylene terephthalate (PET) is one of the most widely used synthetic plastics in the packaging industry, and consequently has become one of the main components of plastic waste found in the environment. However, several microorganisms have been described to encode enzymes that catalyze the depolymerization of PET. While most known PET hydrolases are thermophilic and require reaction temperatures between 60°C and 70°C for an efficient hydrolysis of PET, a partial hydrolysis of amorphous PET at lower temperatures by the polyester hydrolase *IsPETase* from the mesophilic bacterium *Ideonella sakaiensis* has also been reported. We show that polyester hydrolases from the Antarctic bacteria *Moraxella* sp. strain TA144 (Mors1) and *Oleispira antarctica* RB-8 (OaCut) were able to hydrolyze the aliphatic polyester polycaprolactone as well as the aromatic polyester PET at a reaction temperature of 25°C. Mors1 caused a weight loss of amorphous PET films and thus constitutes a PET-degrading psychrophilic enzyme. Comparative modeling of Mors1 showed that the amino acid composition of its active site resembled both thermophilic and mesophilic PET hydrolases. Lastly, bioinformatic analysis of Antarctic metagenomic samples demonstrated that members of the *Moraxellaceae* family carry candidate genes coding for further potential psychrophilic PET hydrolases.

**IMPORTANCE** A myriad of consumer products contains polyethylene terephthalate (PET), a plastic that has accumulated as waste in the environment due to its long-term stability and poor waste management. One promising solution is the enzymatic biodegradation of PET, with most known enzymes only catalyzing this process at high temperatures. Here, we bioinformatically identified and biochemically characterized an enzyme from an Antarctic organism that degrades PET at 25°C with similar efficiency to the few PET-degrading enzymes active at moderate temperatures. Reasoning that Antarctica harbors other PET-degrading enzymes, we analyzed available data from Antarctic metagenomic samples and successfully identified other potential enzymes. Our findings contribute to increasing the repertoire of known PET-degrading enzymes that are currently being considered as biocatalysts for the biological recycling of plastic waste.

**KEYWORDS** Polyethylene terephthalate (PET), polyester hydrolases, plastic biodegradation, *Oleispira antarctica*, *Moraxella* sp., Antarctica, psychrophilic enzymes

**Citation** Blázquez-Sánchez P, Engelberger F, Cifuentes-Anticevic J, Sonnendecker C, Griñén A, Reyes J, Díez B, Guixé V, Richter PK, Zimmermann W, Ramírez-Sarmiento CA. 2022. Antarctic polyester hydrolases degrade aliphatic and aromatic polyesters at moderate temperatures. *Appl Environ Microbiol* 88: e01842-21. <https://doi.org/10.1128/AEM.01842-21>.

**Editor** Haruyuki Atomi, Kyoto University

**Copyright** © 2022 American Society for Microbiology. All Rights Reserved.

Address correspondence to Wolfgang Zimmermann, [wolfgang.zimmermann@uni-leipzig.de](mailto:wolfgang.zimmermann@uni-leipzig.de), or César A. Ramírez-Sarmiento, [cesar.ramirez@uc.cl](mailto:cesar.ramirez@uc.cl).

The authors declare no conflict of interest.

**Received** 16 September 2021

**Accepted** 20 October 2021

**Accepted manuscript posted online** 27 October 2021

**Published** 11 January 2022

Plastics are long-chain synthetic polymers mainly derived from petroleum-based monomers that are widely employed in modern-day applications, such as fibers for clothing and containers for liquids and foods (1). The low cost, malleability, and durability of these polymers has led to the production of ~8,300 million tons of synthetic polymer resins and fibers between 1950 and 2015 (2). The global market for polyethylene terephthalate (PET) is growing and expected to reach 38 billion USD by 2023 (3).

PET waste mismanagement and its resistance to degradation has resulted in a serious threat for the environment (2). Although strategies for waste management and recycling of PET exist, such as thermo-mechanical (i.e., recirculation of plastic waste to produce lower-quality materials) and chemical recycling (i.e., degradation via chemical ester bond cleavage), only a fraction of PET waste is presently recycled (4).

In this context, the discovery of microbial PET-degrading enzymes (5, 6) has emerged as a promising biological approach for plastic recycling (7, 8). These polyester hydrolases are typically cutinases (EC 3.1.1.74) (8) that share a conserved  $\alpha/\beta$ -hydrolase fold and a catalytic triad of amino acids (9). Most enzymes described to date have been derived from thermophilic bacteria and fungi (5, 10) with an optimum activity near the glass transition temperature of PET (~65°C) where the polymer chains become more flexible and prone to enzymatic hydrolysis (11–13).

*IsPETase*, a PET hydrolase from the mesophilic bacterium *Ideonella sakaiensis* 201-F6 has been described to degrade PET with higher efficiency at lower temperatures (20°C to 40°C) than thermophilic cutinases (14). However, the extent of PET degradation by *IsPETase* in this temperature range remained limited compared to hydrolysis by its thermophilic counterparts at their optimum temperature (~65°C) (15).

*IsPETase* has been further studied by several groups, describing that the molecular basis of its activity at moderate temperatures is due to an improved substrate binding at its shallow active site cleft due to the presence of unique residues that enhance PET binding and control active site flexibility (16–19). Importantly, rational design of its active site (17, 20, 21) and its thermostability (22, 23) guided by bioinformatic analysis of currently known PET hydrolases has resulted in up to 300-fold higher activities than the wild-type enzyme.

Most research has been primarily focused on the identification and characterization of thermophilic cutinases, and limited information on other PET hydrolases active at moderate temperatures has been available. A polyester hydrolase from the marine bacterium *Pseudomonas aestusnigri* (24) has also been reported to exhibit limited hydrolytic activity on amorphous PET at 30°C, and variants obtained by rational mutagenesis were also able to release low amounts of mono(2-hydroxyethyl) terephthalate (MHET) from bottle-grade PET. Recent bioinformatic analysis of proteome and metagenome databases has identified 853 potential polyester hydrolases from marine and terrestrial environments including 6 Antarctic enzymes. Among these, an enzyme from *Oleispira antarctica* RB-8 hydrolyzed the aliphatic polyester polycaprolactone (PCL) at room temperature (25).

Psychrophilic microorganisms are interesting candidates as a source of novel enzymes adapted to catalytic activity at low temperatures (26). Hypothesizing that cold-adapted enzymes from such organisms could degrade PET at similar temperatures to *IsPETase* and exhibit differences in residue composition of the active site when compared to thermophilic enzymes, we biochemically characterize two polyester hydrolases from *Oleispira antarctica* RB-8 (OaCut), a psychrophilic oil-degrading bacterium isolated from Antarctic coastal seawater (27) that has already been reported as a PCL hydrolase (25), and a *Moraxella* sp. strain TA144 (Mors1), a bacterium isolated from Antarctic seawater with an optimum growth temperature of 25°C (28).

## RESULTS

### Mors1 and OaCut are polyester hydrolases active at moderate temperatures.

We analyzed the ability of two hydrolases from Antarctic-inhabiting bacteria, Mors1 and OaCut (also identified as PET5 in reference 25), to degrade PCL and PET at moderate

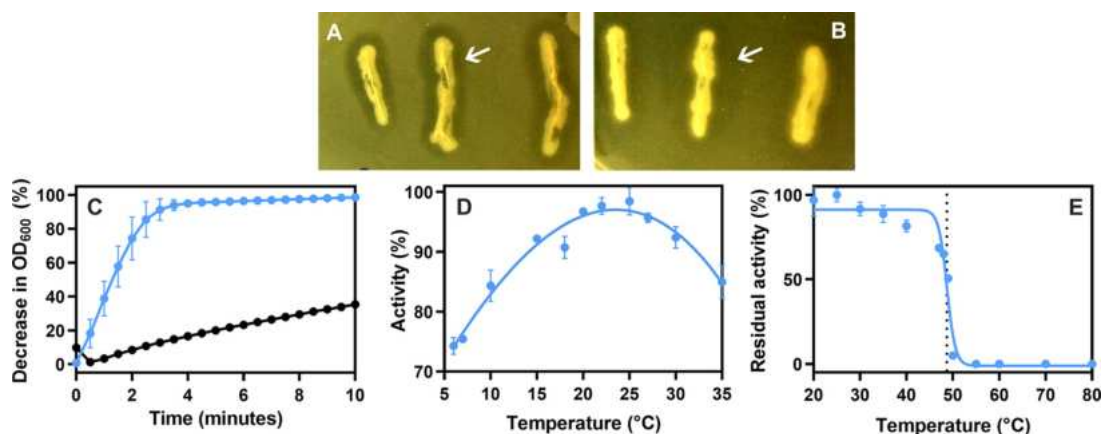


**FIG 1** Hydrolysis of PCL by Mors1 and OaCut. (A) Agar plate containing PCL with *E. coli* expressing Mors1. (B) Agar plate containing PCL with *E. coli* expressing OaCut. (C) Time course of PCL hydrolysis (decrease of turbidity of a PCL nanoparticle suspension) by Mors1 (blue) and OaCut (black). (D) Relative initial hydrolysis rates of PCL nanoparticles by Mors1 at different reaction temperatures; 100% = hydrolysis rate at 25°C. (E) Determination of the thermal inactivation temperature ( $T_{50}$  = 48.7°C) of Mors1.

temperatures. To detect polyester hydrolysis activity of OaCut and Mors1, plate clearing assays were performed with PCL. Overnight incubation at 25°C resulted in the formation of clearing zones around *E. coli* colonies overexpressing Mors1 and OaCut in plates containing PCL (Fig. 1 A–B). These enzymes were then recombinantly expressed and purified (Fig. S1) for enzyme activity and stability analyses.

The PCL-hydrolyzing activity of the two enzymes was compared by measuring the decrease in turbidity of a PCL nanoparticle suspension. Mors1 completely clarified the suspension after a reaction time of 3 min while OaCut decreased the turbidity by only 28% in this time (Fig. 1C).

Analysis of Mors1 by nano differential scanning fluorimetry (nanoDSF) indicated an apparent melting temperature ( $T_m$ ) of 52.0°C and an onset temperature for denaturation of 31.0°C. OaCut showed a  $T_m$  of 40.4°C and an onset temperature for denaturation of 34.8°C (Table 1 and Fig. S2). These values were similar to the  $T_m$  of the mesophilic *IsPETase* (22) and other previously characterized psychrophilic enzymes from *O. antarctica* RB-8, such as the esterase OLEAN\_C09750 with a reported  $T_m$  of 45°C (29).

Using an enzyme concentration of 4.0  $\mu\text{g/ml}$  (0.13  $\mu\text{M}$ ) and a PCL nanoparticle concentration of 0.07 mg/ml, the optimum reaction temperature for PCL hydrolysis by Mors1 was determined as 25°C (Fig. 1D). Mors1 also showed a thermal inactivation temperature ( $T_{50}$ ) of  $48.7 \pm 0.1^\circ\text{C}$  and lost 95% of its PCL-hydrolyzing activity at 50°C (Fig. 1E).

A screening of different reaction buffers showed that the highest PCL-hydrolyzing activity was obtained with sodium phosphate and potassium phosphate buffers at pH 8.0. A further increase of the activity by 20% was observed in the presence of 200 mM NaCl in the reaction mixture (Fig. S3). These results confirm previous reports on the effects of buffer composition and salts on the activity of psychrophilic enzymes (29) and polyester hydrolases (30).

**Kinetic parameters of PCL hydrolysis by Mors1 are similar to *IsPETase*.** When we compared the kinetic parameters for PCL hydrolysis of Mors1 with *IsPETase* and polyester-degrading thermophilic enzymes from *Thermomonospora curvata*, we observed that both Mors1 and *IsPETase* showed a high PCL-hydrolyzing activity (Table 2).

**TABLE 1** Onset temperature for denaturation and melting temperature of Mors1, OaCut, and *IsPETase* determined with nanoDSF

Enzyme	Onset temp for denaturation ( $^\circ\text{C}$ )	$T_m$ ( $^\circ\text{C}$ )
Mors1	$31.0 \pm 0.0$	$52.0 \pm 0.1$
OaCut	$34.8 \pm 0.3$	$40.4 \pm 0.1$
<i>IsPETase</i>	$31.7 \pm 0.3$	$47.1 \pm 0.3$

**TABLE 2** Kinetic parameters of PCL hydrolysis by Mors1, *IsPETase*, Tcur1278, and Tcur0390

Enzyme	$k_r$ ( $10^{-3}/\text{min}^{-1}$ )	$K_A$ (ml/mg)
Mors1	1544 ± 23	152 ± 5
<i>IsPETase</i>	1688 ± 81	94 ± 8
Tcur1278 <sup>a</sup>	122 ± 12	41 ± 5
Tcur0390 <sup>a</sup>	108 ± 6	96 ± 10

<sup>a</sup>Taken from reference 32.

Determination of the kinetic parameters for Mors1 and *IsPETase* (Fig. S4) demonstrated that their apparent hydrolysis rates  $k_r$  and adsorption equilibrium constants  $K_A$  were in a similar range, with *IsPETase* showing 8.5% higher apparent hydrolysis rate and a 38% higher adsorption equilibrium constant for PCL (Table 2). Remarkably, both enzymes showed 13- to 16-fold higher apparent hydrolysis rates and equal or higher adsorption equilibrium constants at 25°C than their thermophilic counterparts near the melting temperature of PCL (60°C) (31, 32).

**Mors1 hydrolyzes amorphous PET films at moderate temperatures.** We further compared the ability of Mors1 and *IsPETase* to hydrolyze amorphous PET films at 25°C. After a reaction time of 24 h with 400 nM (11  $\mu\text{g}/\text{ml}$ ) Mors1 and with 100 nM (2.7  $\mu\text{g}/\text{ml}$ ) *IsPETase* in 1 M potassium phosphate buffer pH 8.0, we observed a 0.59% and 0.46% weight loss of the films for Mors1 and *IsPETase*, respectively (Fig. 2A). These protein concentration and buffer molarity conditions were found to be optimal for the PET hydrolase activity of Mors1 (Fig. S5), the latter being required as the terephthalic acid released during the hydrolysis reaction would considerably lower the pH and alter the enzyme activity otherwise (30). While both enzymes released similar amounts of terephthalic acid (TPA) and MHET, MHET was the main aromatic hydrolysis product of Mors1 at pH 8.0, whereas *IsPETase* produced mainly TPA (Fig. S6). Lower concentrations of Mors1 or higher concentrations of *IsPETase* resulted in a decreased weight loss of the PET films. Similar assays with OaCut showed a lower weight loss of 0.4% compared to Mors1 (1.98%) after a reaction time of 6 days at 25°C (Fig. 2B).

Upon longer reaction times up to 10 days, Mors1 degraded 2.5% of the PET films (Fig. 2C). The surface of the transparent PET films treated with Mors1 for 10 days became

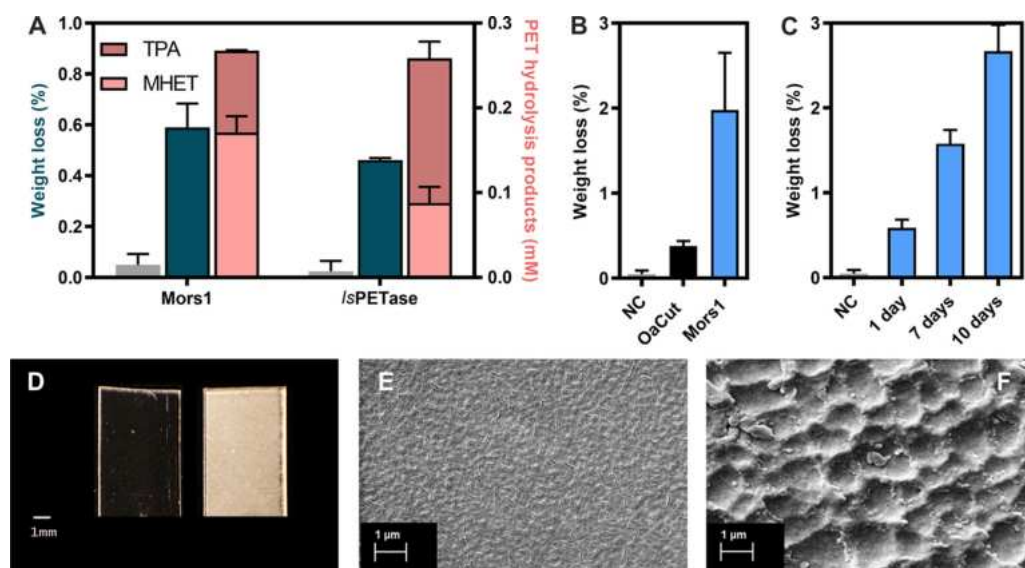


**FIG 2** Enzymatic degradation of amorphous PET films. (A) Weight loss of PET films (in dark green) and amounts of TPA and MHET (in pink) released by Mors1 and *IsPETase* after a reaction time of 24h at 25°C. In gray, negative control without enzyme. (B) Weight loss of PET films after a reaction time of 6 days at 25°C with Mors1 and OaCut. NC: Negative control without enzyme. (C) Weight loss of PET films after a reaction time of 1, 7, and 10 days at 25°C with Mors1. (D) Surface changes of amorphous PET films. A film used as negative control with no enzyme is shown on the left, whereas a film treated with Mors1 for 10 days at 25°C is shown on the right. Scanning electron microscopy images of the surface of an untreated PET film (E) and a film treated with Mors1 for 10 days at 25°C (F).

opaque, indicating an erosion of the surface (Fig. 2D). Analysis by scanning electron microscopy indeed showed the occurrence of pits and grooves on the surface (Fig. 2E and F). Similar effects have previously been observed with other PET-hydrolyzing enzymes (15).

**The active site of Mors1 presents features from mesophilic and thermophilic PET-hydrolyzing cutinases.** Once we established that Mors1 can hydrolyze amorphous PET films at moderate temperatures, we compared the amino acid residue composition of its active site with the mesophilic *IsPETase* and with thermophilic PET hydrolases. We generated a comparative model of Mors1 using Rosetta3 (33) (Fig. S7 and Table S1) and also performed a multiple sequence alignment (MSA) of Mors1 against *IsPETase* (UniProtKB: [A0A0K8P6T7](#)), *OaCut* (UniProtKB: [R4YKL9](#)), *Thermobifida fusca* cutinase (TfCut2, GenBank: [PZN61876.1](#)) and the metagenomic leaf-branch compost cutinase (LCC, UniProtKB: [G9BY57](#)).

Inspection of the MSA (Fig. 3A) and the comparative model of Mors1 (Fig. 3B) showed that Mors1 exhibits features of both mesophilic and thermophilic PET hydrolases. While all enzymes showed a strict conservation of the catalytic triad (S189, D234, H264 in Mors1) and of a Tyr residue (Y121 in Mors1) important for the activity of these enzymes (Fig. 3C) (17), Mors1 contains an additional disulfide bond (C231-C266 in Mors1, DB2 in Fig. 3B) located near the Asp and His residues of the catalytic triad, which is also present in *IsPETase* (C203-C239 in *IsPETase*, Fig. 3A) and in other Type IIa and IIb enzymes, that has been shown to be critical for its hydrolytic activity (17, 18).

The model of Mors1 also revealed a potential third disulfide bridge (C60-C109, DB1 in Fig. 3B) absent in *IsPETase*, which may constitute an adaptation to low temperatures. Fluorescence labeling of free cysteine thiol groups of Mors1 (34) and comparison against a control protein having only one free cysteine suggest that only a small fraction of Mors1 proteins are partially reduced (Fig. S8), thus suggesting that Mors1 could indeed harbor three disulfide bonds. Alas, we were unable to purify single or double mutants of these cysteine residues for further analysis.

While both Mors1 and *IsPETase* also shared the conservation of a Trp residue (W188 in Mors1 and W159 in *IsPETase*), which is substituted by His in thermophilic counterparts, Mors1 carried a Phe residue (F265) that is conserved among PET hydrolases of thermophilic microorganisms and is replaced by Ser in *IsPETase* (Fig. 3A, C, D). Both of these residues have recently been the target for protein engineering of *IsPETase*, leading to a double mutant of this enzyme with improved activity by the addition of His and Phe residues typically found in thermophilic cutinases (21). Furthermore, residues Y214 and Y242 present in Mors1 and in other homologous sequences from psychrophilic organisms corresponded to Trp in all other enzymes, and to His in thermophilic cutinases and Ser in *IsPETase*, respectively (Fig. 3A, C, D). Residue Y242 is highly relevant as structural data has indicated that its substitution by Ser (S214) in *IsPETase* enables the wobbling of its W185 (Y214 in Mors1) that is important for catalysis (16–19).

In previous reports, the ability of *IsPETase* to degrade PET at moderate temperature has been partly explained by its higher active site flexibility when compared to the thermophilic cutinases (18). Thus, we explored the structural flexibility of Mors1 by molecular dynamics (MD) simulations (Fig. 3E). The analysis of several 100 ns MD trajectories of Mors1 showed an overall increase in RMSF mostly in loop regions throughout the whole protein when compared to *IsPETase*. Of particular interest are three regions that conform the active site and its surroundings: 1) the  $\beta$ 6- $\beta$ 7 loop (residues 212–222) where Y214 from subsite I is located, whose equivalent residue in *IsPETase* (the wobbling W185) is crucial for stabilization of the substrate via  $\pi$ - $\pi$  interactions; 2) helix  $\alpha$ 4 and the loops  $\beta$ 7- $\alpha$ 4 and  $\beta$ 8- $\alpha$ 4 (residues 231–251) in Mors1, where the catalytic aspartate is located (D234); and 3) an extended loop (17) composed by residues 260–269, where the catalytic histidine is located (H264), and the beginning of helix  $\alpha$ 5 (residues 269–277).

**Identification of polyester hydrolases from Antarctic marine environments.** To identify further potential polyester hydrolases from Antarctic marine environments, we assembled two marine metagenomes from Chile Bay (Greenwich Island) in Antarctica (NCBI: BioProject no. [PRJNA421008](#)) (35) using SPAdes (36): One was corresponding to



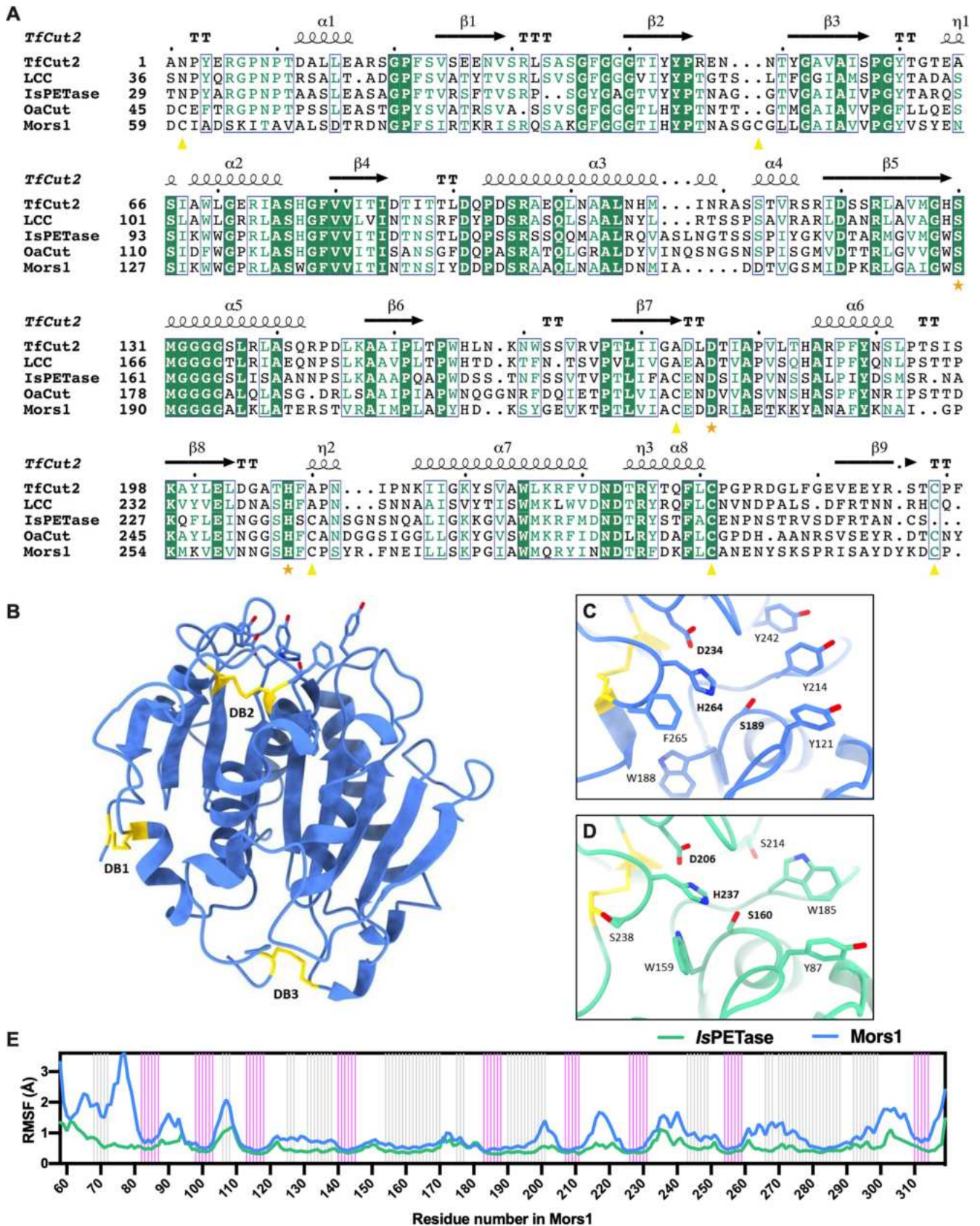


**FIG 3** Comparison of the sequence, structure, and active site dynamics of *Mors1*, *OaCut*, *IsPETase*, *TfCut2*, and LCC. (A) Multiple sequence alignment. Residues numbered according to the full protein sequences with signal peptide. Strictly conserved residues are highlighted in green background, with (Continued on next page)

a condition of low productivity, based on the concentration of chlorophyll *a* (Low Chl*a*), and the second was corresponding to a condition of high productivity during a phytoplankton bloom recorded in the austral summer of 2014 in Chile Bay (High Chl*a*). Once we obtained all predicted proteins from these metagenomes using Prodigal (37), we used the full-length amino acid sequence of Mors1 (UniProtKB P19833) as reference to identify homologs from these predicted Antarctic metagenome proteins using BLASTP (38).

This analysis led to the identification of 6 enzymes having 71–90% sequence identity and 56–97% sequence coverage in both metagenomes (Table S2 and Fig. 4). When analyzing the source contigs, we observed that the proteins with lower sequence coverage (mtgmn1, mtgmn3) were truncated not by the presence of terminal codons, but because the contig was terminated before a protein termination signal could be identified. Moreover, bioinformatic analysis using SignalP (39) identified a signal peptide in 4 of these enzymes (mtgmn1, mtgmn3, mtgmn4, mtgmn6), which is consistent with what has been observed for all characterized PET hydrolases to date. Regarding the taxonomic affiliation of these enzymes, BLAST analysis against the RefSeq protein database showed that they had high sequence identity (>82%) with proteins of the genus *Psychrobacter* of the *Moraxellaceae* family (Table S3). The difference in the taxonomic assignment of these enzymes to the genus *Psychrobacter* and not to the genus *Moraxella* could be explained by a possibly erroneous sequence annotation of Mors1, which was taxonomically classified using biochemical tests and not genome phylogeny analysis.

When evaluating the relative abundance of the taxa that potentially carry these sequences in the Antarctic metagenomes, we determined that the *Moraxellaceae* family represented ~40% of the total reads assigned as 16S rRNA genes in the Low Chl*a* metagenome. Meanwhile, in the High Chl*a* metagenome, the reads assigned to the *Moraxellaceae* family represented only ~3% of the total. These values were in good agreement with those reported previously (40), where Pseudomonadales (to which *Moraxella* and *Psychrobacter* genera belong) was the dominant marine order in a low Chl*a* metagenome, and then Alteromonadales order dominated in a high Chl*a* metagenome obtained during the phytoplankton bloom recorded in Chile Bay in 2014. Using Bowtie2 (41), we determined that the Mors1 homologs recruit only 0.0005% and 0.0001% of the total number of reads from the Low and High Chl*a* metagenomes, respectively. This low abundance, compared to the relative abundance of 16S rRNA genes of the *Moraxellaceae* family members, indicates that not all members of this family are carriers of these candidate enzymes.

## DISCUSSION

We characterized two psychrophilic polyester hydrolases, Mors1 and OaCut from the Antarctic bacteria *Moraxella* sp. TA144, and *Oleispira antarctica* RB-8, respectively, demonstrating their ability to hydrolyze both aliphatic and aromatic polyester at moderate temperatures. Both enzymes hydrolyzed the aliphatic polyester PCL and the aromatic polyester PET, with Mors1 showing a higher activity. While the degradation of PCL by OaCut has been reported previously, a hydrolysis of PET has not been observed in a plate clearing assay (25).

The hydrolysis of PCL at 30°C by a lipase from *Moraxella* sp. TA144 (MorEst) has also been reported (42). A weight loss of 18% after 3 days of reaction was achieved in a mixture containing 10 mg/ml of powdered PCL with 25 mg of enzyme and a further addition of 12 mg of MorEst 24 and 48 h later. MorEst also hydrolyzed bis(2-hydroxyethyl) terephthalate and a PET dimer, but a commercial PET sample was not hydrolyzed. Since the

### FIG 3 Legend (Continued)

yellow triangles indicating cysteine pairs that form disulfide bonds and orange stars indicating catalytic residues. A secondary structure topology based on the structure of *TfCut2* (PDB 4CG1) is shown on top of the sequence alignment. (B) Cartoon representation of the modeled structure of Mors1, showing its three disulfide bridges (DB) in yellow sticks. (C) Active site of Mors1 (blue), with catalytic residues in bold. (D) Active site of *IsPETase* (green), showing residues equivalent to Mors1 and catalytic residues in bold. (E) Average backbone RMSF for Mors1 and *IsPETase*. The secondary structure is indicated as lines in the background, with  $\alpha$ -helices in pink and  $\beta$ -sheets in gray.



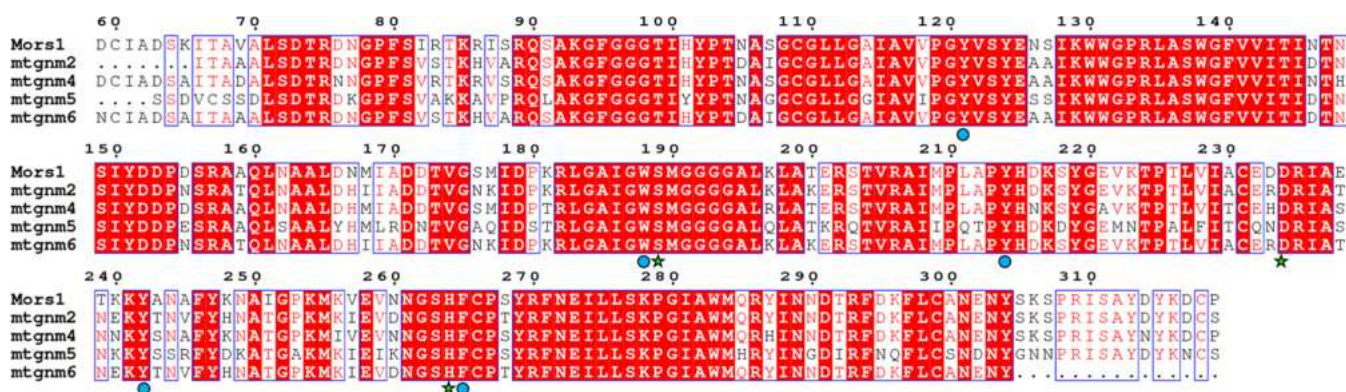


**FIG 4** Sequence variability of potential polyester hydrolases from Antarctic metagenomes. A multiple sequence alignment between Mors1 and homologous enzyme candidates with high sequence coverage from Antarctic metagenomes from Chile Bay. Blue boxes indicate columns with either strict (red background) or 75% (red characters) sequence conservation between all enzymes. Green stars indicate conserved catalytic residues, whereas blue spheres indicate active site residues.

sequence of the enzyme was not communicated, the identity of MorEst with Mors1 could not be determined.

It has been previously demonstrated that polyester hydrolases, for example the metagenomic leaf-branch compost cutinase LCC or Tcur1278 and Tcur0390 from the thermophilic actinomycete *Thermomonospora curvata* efficiently degraded PCL at a reaction temperature of about 50°C (13, 32). *IsPETase* has been described not to be able to degrade aliphatic polyesters such as polybutylene succinate and polylactic acid (21). In contrast, we found that *IsPETase* showed kinetic parameters similar to Mors1 hydrolyzing the aliphatic polyester PCL at pH 8.0 at a reaction temperature of 25°C. Mors1 showed a considerably higher PET-degrading activity than OaCut. Mors1 caused a weight loss of amorphous PET films and released PET hydrolysis products at optimum reaction conditions in the same range as the mesophilic *IsPETase*, demonstrating the ability of Antarctic psychrophilic enzymes to degrade PET. It is worth noting that the activity of *IsPETase* can be further increased by about 3-fold at pH 9.0 (14).

A classification of PET hydrolases based on their amino acid residue conservation in subsites I and II within the active site of these enzymes (17) enabled to categorize OaCut as a Type IIa enzyme due to its residue composition (L105, L106, W176, F256, F259 in subsite II). In contrast, Mors1 presented differences in both subsites (D153, Y214 in subsite I; V122, S123, W188, F265, S268 in subsite II), which impedes its unambiguous classification under any of the Type I, IIa or IIb categories. These results suggest that the composition of the active site of these polyester hydrolases is more diverse than previously considered.

Computational analysis of the sequence and structure of Mors1 suggested that its ability to hydrolyze PCL and amorphous PET at moderate temperatures is due to features that this enzyme shares with both thermophilic PET hydrolases and the mesophilic *IsPETase*. The presence of a disulfide bond near the active site, absent in thermophiles but equivalent to the one found in Type II enzymes (17), was a prominent indicator that Mors1 could also show polyester-hydrolyzing activity at moderate temperatures. In *IsPETase*, this disulfide bond compensates the increased structural flexibility of its active site while keeping the integrity of the catalytic triad. An opening of the disulfide bond decreased the  $V_{max}$  for the hydrolysis of *p*-nitrophenyl acetate by almost 28% (18) and its replacement by alanine causing a  $T_m$  drop of 13.2°C (17). Our MD simulations provided evidence that Mors1 also possesses a highly flexible active site, which could explain its activity at 25°C. Our analysis suggested the presence of a further disulfide bond (C60-C109) in Mors1, which could also correspond to the stabilization strategy of psychrophilic and psychrotropic organisms to counterbalance the additional flexibility on the structure of their enzymes (43).

The increased flexibility of regions that contain both catalytic and substrate binding residues could be indicative of enthalpic–entropic tradeoffs to enable PET hydrolysis at



moderate temperatures, as it has been shown for other cold-active enzymes (43). However, further docking experiments followed by MD simulations are required to analyze such tradeoffs in the active site of Mors1.

Reasoning that there could be more enzymes from Antarctic microorganisms catalyzing the hydrolysis of polyesters at moderate temperatures, and taking into account recent bioinformatic analysis of proteome and metagenome databases that identified 6 Antarctic enzymes among 853 potential PET hydrolases from marine and terrestrial environments (25), we performed a metagenomic analysis of Antarctic marine environments. The results provided evidence for the presence of further potential polyester hydrolases homologous to Mors1 with likely similar activities in Antarctic coastal waters, specifically in members of the family *Moraxellaceae*. Among 6 new enzymes identified with moderate to high identity to Mors1, we observed a localized sequence variability in regions near the active site residues, which suggested potential differences in their polyester-hydrolyzing activity. No homologous Antarctic enzymes were detected outside this family, which could be due to a specific niche inhabited by some members of the *Moraxellaceae* family. The low abundance of the enzyme sequences in Antarctic metagenomes compared to the relative abundance of the *Moraxellaceae* family members in the bacterial marine community suggests a possible niche function of members of this family in using these hydrolases.

Although *IsPETase* and Mors1 catalyzed the hydrolysis of amorphous PET at moderate temperatures, their hydrolysis rates remained low when compared to thermophilic cutinases at higher temperatures. Due to the stiffness of the PET polymer below its glass transition temperature, an extensive degradation of PET cannot be expected at 25°C (44). However, in applications requiring a limited hydrolysis of PET at moderate temperatures, for example in laundry detergents for synthetic textiles (45), the Antarctic psychrophilic polyester hydrolases have the potential to become valuable industrial biocatalysts in the future.

Determining the existence of metabolic pathways to assimilate PET degradation products in Antarctic microorganism communities (46) could give further clues as to whether there is an evolutionary adaptation of microorganisms to consume PET in the environment or if the ability of the described enzymes to hydrolyze PET is rather due to their unusual broad substrate specificity.

Our results established that Mors1 and OaCut are polyester hydrolases able to hydrolyze both aliphatic and aromatic polyesters at moderate temperatures. Sequence comparison analysis showed that the active site of Mors1 contained features of both the mesophilic *IsPETase* and thermophilic enzymes. Metagenomic analysis of Antarctic seawater samples enabled the identification of potential further PET hydrolases of the *Moraxellaceae* family, their abundance in the marine community, and sequence variations. Altogether, our results describe an Antarctic psychrophilic enzyme that degrades amorphous PET at moderate temperatures, furthering our understanding of the sequence variations that have allowed the emergence of this catalytic activity in nature.

## MATERIALS AND METHODS

**Bioinformatic identification of OaCut and Mors1.** A BLAST (38) search against the UniProt Knowledgebase (UniProtKB (47)) was performed using the amino acid sequence of *IsPETase* (UniProtKB [A0A0K8P6T7](#)) as a query, identifying the sequences of OaCut (UniProtKB [R4YKL9](#), 53% sequence identity) and Mors1 (UniProtKB [P19833](#), 45% sequence identity). N-terminal signal peptides and disordered regions were removed using SignalP (39) and PrDOS (48), respectively.

**Protein expression and purification.** Codon-optimized genes encoding truncated Mors1 (residues 59–319) and OaCut (residues 47–310) were synthesized (Genscript, Piscataway, NJ, USA), cloned into a pET28a vector (EMD Biosciences, Madison, WI, USA) as NdeI/BamHI fragments and transformed into *Escherichia coli* BL21(DE3). The bacteria were grown in kanamycin-supplemented Terrific Broth medium (Thermo Fisher Scientific, Waltham, MA, USA). Upon reaching  $OD_{600} = 0.6$ , protein expression was induced with 1 mM isopropyl  $\beta$ -D-1-thiogalactopyranoside (IPTG) and the bacterial culture was further grown for 16 h at 14°C. Cells were harvested by centrifugation and then lysed by sonication in buffer containing 50 mM sodium phosphate pH 8.0, 200 mM NaCl, and 8 M urea. A cleared lysate was collected by centrifugation and loaded onto a Ni-Sepharose resin (HisTrap FF crude, GE Healthcare Life Sciences, Pittsburgh, PA, USA). To remove urea, His-tagged protein was dialyzed overnight at 4°C and then loaded onto a HiLoad Superdex 200 prep grade size exclusion chromatography column (GE Healthcare Life

Sciences) using an ÄKTA pure FPLC (GE Healthcare Life Sciences). The purity of the preparations was confirmed by sodium dodecyl sulfate-polyacrylamide gel electrophoresis (SDS-PAGE) (Fig. S1). Protein concentration was determined by the Bradford assay (49) (ROTI Quant, Carl Roth GmbH + Co. KG, Karlsruhe, Germany).

**PCL plate clearing assays.** PCL nanoparticle suspension was prepared as previously described (32, 50, 51). Plate clearing assays were performed to preliminarily ascertain if OaCut and Mors1 degrade PCL (51). For the preparation of PCL agar plates, nanoparticle suspensions of PCL were added to autoclaved LB-agar (6% vol/vol) at 60°C supplemented with 0.5 mM IPTG and 37  $\mu\text{g/ml}$  kanamycin. Recombinant *E. coli* cells harboring the pET28a-OaCut and pET28a-Mors1 plasmids were inoculated onto the plates and incubated at room temperature up to 4 days. The formation of a clearing zone around colonies was used as indication of PCL-hydrolyzing activity (25).

**Thermal stability of OaCut and Mors1.** The apparent melting temperature ( $T_m$ ) of OaCut and Mors1 was determined using nano-differential scanning fluorimetry (nanoDSF, Prometheus NT.48, Nanotemper Technologies, Munich, Germany). A thin glass capillary was filled with purified Mors1 and OaCut at a concentration of 150  $\mu\text{g/ml}$  in 20 mM HEPES pH 7.5, 70 mM NaCl, and heated from 20°C to 95°C with a slope of 1°C/min (Fig. S2). The intrinsic fluorescence emission of tryptophan residues was measured at 330 and 350 nm, and the first derivative of the ratio of fluorescence at 330 and 350 nm was calculated to obtain the apparent  $T_m$ .

**Determination of optimum reaction temperature and buffer conditions for PCL hydrolysis by Mors1.** To determine optimum reaction temperature and buffer conditions for the hydrolysis of PCL by Mors1, the hydrolysis rates were determined by monitoring the decrease in turbidity of a PCL nanoparticle suspensions as previously described (32, 52). The reaction mixtures contained buffer and purified Mors1 (4.0  $\mu\text{g/ml}$ ) in a total volume of 200  $\mu\text{l}$ . The reaction was started by the addition of 0.07 mg/ml PCL nanoparticle suspension. Initial hydrolysis rates were determined from the linear part of the graphs of decreasing OD<sub>600</sub> over time. Experiments were performed in triplicates. To determine the optimum reaction temperature for the hydrolysis of PCL by Mors1, initial hydrolysis rates were measured at reaction temperatures between 5°C and 35°C in 20 mM HEPES pH 7.5 every 6 s using a Cary 60 UV-Vis spectrophotometer (Agilent Technologies, Santa Clara, CA, USA). To determine the optimum NaCl concentration for the hydrolysis of PCL by Mors1, hydrolysis rates were measured in 20 mM HEPES pH 7.5 buffer supplemented with NaCl in concentrations of 100, 200, and 500 mM. PCL hydrolysis rates were determined after 1, 3, and 24 h of incubation at 25°C. The enzyme activity determined after 1 h of incubation in 20 mM HEPES pH 7.5 buffer was set to 100%.

The half-inactivation temperature of Mors1 ( $T_{50}$ ), i.e., the temperature at which the enzyme activity was reduced by 50% in relation to its activity at 25°C, was determined by incubating 3.0  $\mu\text{g/ml}$  Mors1 for 15 min in 125 mM sodium phosphate buffer pH 8.0 containing 200 mM NaCl at temperatures from 20°C to 80°C. The residual activity was determined at 25°C by measuring the hydrolysis rates of PCL nanoparticles. The data were fitted to a sigmoidal Boltzmann regression curve and the  $T_{50}$  value was obtained by determination of the inflection point.

The effect of five buffers (sodium phosphate, Bis-Tris, HEPES, Tris, and potassium phosphate) at pH 7.0 and 8.0 (Tris also at pH 9.0) on the hydrolysis of PCL nanoparticles by Mors1 was compared by reacting 4.0  $\mu\text{g/ml}$  Mors1 with 0.07 mg/ml PCL nanoparticles in 125 mM the corresponding buffer supplemented with 200 mM NaCl for 1, 3, and 72 h at 25°C. Hydrolysis rates determined after 1 h in 20 mM HEPES pH 7.5. The enzyme activity determined at 200 mM NaCl was set to 100%.

**Kinetic parameters of PCL hydrolysis by Mors1.** To determine the kinetic parameters of the PCL hydrolysis reaction catalyzed by Mors1 and *IsPETase*, assays were performed at 25°C in a reaction mixture containing 125 mM sodium phosphate pH 8.0, 200 mM NaCl and 0.07 mg/ml PCL nanoparticles with varying enzyme concentrations from 0.6 to 22.0  $\mu\text{g/ml}$ . Optimal buffer conditions for these assays (Fig. S3) were determined as described above. Assays were performed in triplicates using 96-well microplates, measuring the change in turbidity at OD<sub>600</sub> in 10 sec intervals for a total reaction time of 10 min with a Synergy HTX multi-mode microplate reader (Biotek Instruments Inc, Winooski, VT, USA). The kinetic parameters were determined with a pseudo-first order kinetic equation (32, 52) (Fig. S4).

**Hydrolysis of amorphous PET films by Mors1, OaCut, and *IsPETase*.** Amorphous PET films with a size of 0.5 cm  $\times$  3 cm (~45 mg) (250  $\mu\text{m}$  thickness; product number ES301445, Goodfellow, Hamburg, Germany) were incubated with 1 M potassium phosphate pH 8.0, 200 mM NaCl and 400 nM Mors1, 400 nM OaCut and 100 nM *IsPETase* at 25°C for 24 h with shaking. The PET films were collected, washed with water, aqueous SDS (0.5%) and ethanol, dried at 50°C overnight and weighted to determine the weight loss gravimetrically. Hydrolysis reactions were also performed for 6, 7, and 10 days with 400 nM Mors1 and for 6 days with 400 nM OaCut.

The soluble PET hydrolysis products MHET and TPA, present in the supernatants of 24 h reactions of the PET films with the enzymes, were analyzed by HPLC using a C18 column (Eurospere II 100-5; 150  $\times$  2 mm with pre-column, Knauer Wissenschaftliche Geräte GmbH, Berlin, Germany) at a flow rate of 0.3 ml/min on an Agilent 1100 Series HPLC instrument (Agilent Technologies, La Jolla, CA, USA). The mobile phase consisted of acetonitrile with 0.1% formic acid (A) and 0.1% formic acid (B). A gradient was performed as follows: 95% B (0.0 min), 80% B (0.1 min), 76% B (3.0 min), 60% B (3.1 min), 0% B (8.0 min), hold for 2 min and back to 95% B (analysis time 12.0 min). The injection volume of the sample was 2  $\mu\text{l}$  and the separated products were detected by their absorbance at 241 nm. TPA (Sigma-Aldrich, St. Louis, MO, USA) and MHET were used as standard. MHET was synthesized as described elsewhere by the hydrolysis of bis(hydroxyethyl) terephthalate (BHET) (Sigma-Aldrich, St. Louis, MO, USA) with KOH (53). Trimesic acid (TMA) (Sigma-Aldrich, St. Louis, MO, USA) was used as internal standard. The amount of

PET film per microliter of the reaction volume (0.025 mg PET/ $\mu$ l reaction) was identical as described for the analysis of *IsPETase* (14).

**Scanning electron microscopy of PET films.** PET films fixed on glass substrates were analyzed on a scanning electron microscope (EVO LS10, Carl Zeiss GmbH, Germany) with a LAB6 cathode (Kimball Physics, NH, USA) and a secondary electron detector. PET films were sputter-coated using a BAL-TEC model SCD 050 (Leica Biosystems, Wetzlar, Germany) with 25 nm gold prior to imaging. Images were captured at an acceleration voltage of 7 kV and a probe current of 5 pA.

**Comparative modeling of Mors1.** A comparative model for Mors1 was generated by first selecting high-sequence identity structure templates through a BLAST search against the Protein Data Bank (54). The solved crystal structures of *IsPETase* (PDB 6EQE) (21), the cutinases from *Thermobifida cellulosilytica* (PDB 5LUI) (55) and *Thermobifida fusca* (PDB 4CG2) (56), and a polyester hydrolase of *Pseudomonas aestuvaria* (PDB 6SBN) (24) were selected.

Chain A of each structure was extracted and used as template alongside a RosettaScripts XML modeling protocol (57) to generate a total of 1,000 models, where explicit information about the position of the two conserved disulfide bonds and an additional bond were obtained according to the cysteine residues present in the sequence. The lowest-energy model with the lowest RMSD against the template structures was selected and its stereochemical quality was assessed using Verify3D(58), PROVE (59), PROCHECK (60), and WHATCHECK (61). Further refinement of this structure was conducted using two custom relax protocols (62) with and without restraints on the active site, generating 5,000 additional models that underwent a similar energetical and structural quality assessment for selection of a final model.

The five models with lowest-energy and RMSD against the template structure of *IsPETase* (PDB 6EQE) were selected for further analysis (Table S1 and Fig. S7). We did not observe significant differences in the Ramachandran plots for the models 119, 620, 650, 803, and 952. Only 2 amino acids, excluding glycine, were in the non-favored regions, similar to the structure of *IsPETase*, which presented one residue in a non-favored region, corresponding to serine 132.

With Verify3D(58), which determines the compatibility of the model with its own primary sequence based on known protein structures, we obtained positive values for all the models, with models 119 and 650 showing the best results. With PROVE, better results were obtained for model 952 with a buried outlier protein atom total of 3.6%. Considering WHATCHECK results, the model 199 showed less errors in comparison to the others and displayed a properly oriented catalytic triad as in the template structures. Thus, model 119 was selected, and 5,000 relaxed models were generated. No improvements were obtained, indicating a good quality of the model 119.

**Molecular dynamics simulations.** Molecular dynamic (MD) simulations with Mors1 and *IsPETase* (PDB 6EQE) were carried out using AMBER16 along with the ff14SB force field (63). The protonation state of the residues at pH 8.0 was estimated using the H++ server (64). Then, a system was solvated with TIP3P water molecules and neutralized with counter ions in a truncated octahedral box of 1.5 nm of padding with periodic boundary conditions. The system was first minimized using a steepest descent method with position restraints on waters and ions, followed by a second minimization without any position restraints. The system was heated from 0 to 298 K for 150 ps at a constant volume using a Langevin thermostat, followed by equilibration of the solvent atoms of each system for 1 ns at 298 K and constant pressure of 1 bar using a Berendsen barostat until density was stable, upon which a third and final equilibration step of the whole system for 1 ns under the same temperature and pressure conditions was performed. Production MD runs were carried out in four replicas for 100 ns each, using a timestep of 2.0 fs alongside the SHAKE (65) algorithm and the particle mesh Ewald method (66) for long-range electrostatics, with a 10 Å cutoff for short-range electrostatics. Independent runs were ensured by using random seeds for initial velocities during the equilibration step. Replicas were checked for structural convergence using the overall backbone root mean-square deviation (RMSD) from the first frame. RMSD and per-residue root mean square fluctuations (RMSF) were calculated using CPPTRAJ of AmberTools20 (67).

**Fluorescent dye labeling of free cysteines in Mors1.** The presence of free thiol groups of cysteine residues in Mors1 was determined by covalent labeling with the fluorescent dye 7-fluoro-2,1,3-benzoxadiazole-4-sulfonamide (ABD-F) (34). Both Mors1 and BSA were adjusted to equal molar concentrations, and 4  $\mu$ l of protein was mixed with 5  $\mu$ l of 2 $\times$  reaction buffer (200 mM H<sub>3</sub>BO<sub>3</sub>, 4 mM EDTA, 6% SDS, pH 8.0) and 1  $\mu$ l of 10 $\times$  ABD-F (40 mM in DMSO) and incubated for 30 min at 37°C (Fig. S8). Labeled samples were separated on an SDS-PAGE gel under non-reducing conditions, and fluorescence was detected in a ChemiDoc XRS+ Gel Imaging System (Bio-Rad Laboratories, Hercules CA, USA). BSA was used as a positive control since it contains 35 cysteine residues that form 17 disulfide bridges and one free cysteine which can be covalently labeled with ABD.

**Identification of potential PET hydrolases in Antarctic coastal metagenomes.** Genes encoding Mors1 homologs were identified from massive sequencing data obtained in 2014 from surface marine waters of Bahía Chile, Antarctica (35), available at the NCBI BioProject no. PRJNA421008. Metagenome readings were filtered using a quality score (Qscore) > 30 and assembled with the SPAdes v3.10.1 software using the “meta” option (36). The prediction of open reading frames (ORFs) was made from contigs greater than 500 bp with Prodigal v2.6.3 using the “meta” mode and bypassing the Shine-Dalgarno sequence (37). Lastly, potential polyester hydrolases from the predicted proteins of these metagenomes were identified via local sequence homology analysis against the protein sequence of Mors1 (UniProtKB P19833) using BLASTP (38), with hits having > 50% coverage and > 70% sequence identity considered valid.

**Abundance and taxonomic affiliation of potential metagenomic PET hydrolases.** The composition of the bacteria community was evaluated through 16S miTAG analysis, which was obtained and recorded from metagenomes using METAXA2 (68) in metagenomic mode using default parameters.



Recruitment of readings to the sequences of potential Mors1 homologs was carried out through the use of Bowtie2 v2.2.6 (41) in the end-to-end alignment mode and allowing 1 mismatch in a seed alignment during multiseed alignment. Then, we identified the possible taxonomic identity of the candidate metagenome sequences through BLASTP (38) against the Refseq\_prot database (NCBI, January 2020). Only the best hit was reported, since the first 10 results corresponded to the same taxonomy.

**Data availability.** The results from comparative modeling of Mors1 using Rosetta, MD simulations of *IsPETase* and Mors1 and homologous metagenomic sequences identified from NCBI BioProject no. PRJNA421008 are available for download at the laboratory's simulation archive in the Open Science Framework (OSF, <https://osf.io/bn6u3/>). The protein sequences of *IsPETase*, OaCut, and Mors1 are available at the UniProt KB under accession codes A0A0K8P6T7 (*IsPETase*), R4YKL9 (OaCut), and P19833 (Mors1).

## SUPPLEMENTAL MATERIAL

Supplemental material is available online only.

**SUPPLEMENTAL FILE 1**, PDF file, 1.3 MB.

## ACKNOWLEDGMENTS

This research was funded by Instituto Antártico Chileno (INACH Regular Grant RG\_47\_16 to C.A.R.-S. and Doctoral Thesis Support Grant DG\_11\_18 to P.B.-S.), the National Agency for Research and Development (ANID) from Chile and the Sao Paulo State Foundation for Research (FAPESP) from Brazil (ANID-FAPESP PCI 2019/13259-9), and the ANID—Millennium Science Initiative Program—ICN17\_022. P.B.-S. and J.R. were funded by ANID Doctoral Scholarships (21191979 and 21191684, respectively). C.S. was funded by the Biotechnology and Biological Sciences Research Council (BB/T011289/1). B.D. was funded by DPI, grant number DPI20140044-ANID. Powered@NLHPC: This research was partially supported by the supercomputing infrastructure of the NLHPC (ECM-02).

We thank Ronny Frank from the Centre for Biotechnology and Biomedicine, Molecular Biological-Biochemical Processing Technology of Leipzig University for providing the SEM images.

We declare no conflicts of interest.

P.B.-S., B.D., W.Z., C.A.R.-S.: conceptualization. P.B.-S., F.E., J.C.-A., C.S., B.D., W.Z., C.A.R.-S.: methodology. P.B.-S., F.E., J.C.-A., A.G., C.S., P.K.R., J.R.: investigation. P.B.-S., F.E., J.C.-A., B.D., C.A.R.-S.: formal analysis. P.B.-S., F.E., J.C.-A., B.D., V.G., W.Z., C.A.R.-S.: writing—original draft. P.B.-S., B.D., V.G., W.Z., C.A.R.-S.: writing—review and editing. P.B.-S., C.S., B.D., V.G., C.A.R.-S.: funding acquisition.

## REFERENCES

- Scott G. 2006. Polymers in modern life, p 1–18. *In* Scott G (ed), *Polymers and the environment*. RSC Publishing, London, UK.
- Jambeck JR, Geyer R, Wilcox C, Siegler TR, Perryman M, Andrady A, Narayan R, Law KL. 2015. Plastic waste inputs from land into the ocean. *Science* 347: 768–771. <https://doi.org/10.1126/science.1260352>.
- Satsangi S. 2017. Polyethylene terephthalate (PET) market by application (beverages, sheet & films, consumer goods, food packaging, and others) and end-use industry (packaging, electrical & electronics, automotive, construction, and others): global opportunity analysis and industry forecast, 2017–2023. Big Market Research, Portland, OR, USA.
- García JM, Robertson ML. 2017. The future of plastics recycling. *Science* 358:870–872. <https://doi.org/10.1126/science.aaq0324>.
- Kawai F, Kawabata T, Oda M. 2019. Current knowledge on enzymatic PET degradation and its possible application to waste stream management and other fields. *Appl Microbiol Biotechnol* 103:4253–4268. <https://doi.org/10.1007/s00253-019-09717-y>.
- Taniguchi I, Yoshida S, Hiraga K, Miyamoto K, Kimura Y, Oda K. 2019. Biodegradation of PET: current status and application aspects. *ACS Catal* 9: 4089–4105. <https://doi.org/10.1021/acscatal.8b05171>.
- Zimmermann W. 2020. Biocatalytic recycling of polyethylene terephthalate plastic: Biocatalytic plastic recycling. *Philos Trans A Math Phys Eng Sci* 378:1–7.
- Wei R, Zimmermann W. 2017. Biocatalysis as a green route for recycling the recalcitrant plastic polyethylene terephthalate. *Microb Biotechnol* 10: 1302–1307. <https://doi.org/10.1111/1751-7915.12714>.
- Lenfant N, Hotelier T, Velluet E, Bourne Y, Marchot P, Chatonnet A. 2013. ESTHER, the database of the  $\alpha/\beta$ -hydrolase fold superfamily of proteins: tools to explore diversity of functions. *Nucleic Acids Res* 41:D423–D429. <https://doi.org/10.1093/nar/gks1154>.
- Wei R, Zimmermann W. 2017. Microbial enzymes for the recycling of recalcitrant petroleum-based plastics: how far are we? *Microb Biotechnol* 10:1308–1322. <https://doi.org/10.1111/1751-7915.12710>.
- Ronkvist ÅM, Xie W, Lu W, Gross RA. 2009. Cutinase-catalyzed hydrolysis of poly(ethylene terephthalate). *Macromolecules* 42:5128–5138. <https://doi.org/10.1021/ma9005318>.
- Mueller RJ. 2006. Biological degradation of synthetic polyesters—enzymes as potential catalysts for polyester recycling. *Process Biochem* 41: 2124–2128. <https://doi.org/10.1016/j.procbio.2006.05.018>.
- Sulaiman S, Yamato S, Kanaya E, Kim J-J, Koga Y, Takano K, Kanaya S. 2012. Isolation of a novel cutinase homolog with polyethylene terephthalate-degrading activity from leaf-branch compost by using a metagenomic approach. *Appl Environ Microbiol* 78:1556–1562. <https://doi.org/10.1128/AEM.06725-11>.
- Yoshida S, Hiraga K, Takehana T, Taniguchi I, Yamaji H, Maeda Y, Toyohara K, Miyamoto K, Kimura Y, Oda K. 2016. A bacterium that degrades and assimilates poly(ethylene terephthalate). *Science* 351:1196–1199. <https://doi.org/10.1126/science.aad6359>.
- Wei R, Breite D, Song C, Gräning D, Ploss T, Hille P, Schwerdtfeger R, Matysik J, Schulze A, Zimmermann W. 2019. Biocatalytic degradation efficiency of postconsumer polyethylene terephthalate packaging determined by their polymer microstructures. *Adv Sci (Weinh)* 6:1900491. <https://doi.org/10.1002/advs.201900491>.
- Han X, Liu W, Huang J-W, Ma J, Zheng Y, Ko T-P, Xu L, Cheng Y-S, Chen C-C, Guo R-T. 2017. Structural insight into catalytic mechanism of PET hydrolase. *Nat Commun* 8:2106. <https://doi.org/10.1038/s41467-017-02255-z>.

17. Joo S, Cho IJ, Seo H, Son HF, Sagong HY, Shin TJ, Choi SY, Lee SY, Kim KJ. 2018. Structural insight into molecular mechanism of poly(ethylene terephthalate) degradation. *Nat Commun* 9:382. <https://doi.org/10.1038/s41467-018-02881-1>.
18. Fecker T, Galaz-Davison P, Engelberger F, Narui Y, Sotomayor M, Parra LP, Ramírez-Sarmiento CA. 2018. Active site flexibility as a hallmark for efficient PET degradation by *I. sakaiensis* PETase. *Biophys J* 114:1302–1312. <https://doi.org/10.1016/j.bpj.2018.02.005>.
19. Liu B, He L, Wang L, Li T, Li C, Liu H, Luo Y, Bao R. 2018. Protein crystallography and site-direct mutagenesis analysis of the poly(ethylene terephthalate) hydrolase PETase from *Ideonella sakaiensis*. *Chembiochem* 19:1471–1475. <https://doi.org/10.1002/cbic.201800097>.
20. Ma Y, Yao M, Li B, Ding M, He B, Chen S, Zhou X, Yuan Y. 2018. Enhanced poly(ethylene terephthalate) hydrolase activity by protein engineering. *Engineering* 4:888–893. <https://doi.org/10.1016/j.eng.2018.09.007>.
21. Austin HP, Allen MD, Donohoe BS, Rorrer NA, Kearns FL, Silveira RL, Pollard BC, Dominick G, Duman R, El Omari K, Mykhaylyk V, Wagner A, Michener WE, Amore A, Skaf MS, Crowley MF, Thorne AW, Johnson CW, Woodcock HL, McGeehan JE, Beckham GT. 2018. Characterization and engineering of a plastic-degrading aromatic polyestherase. *Proc Natl Acad Sci U S A* 115:E4350–E4357. <https://doi.org/10.1073/pnas.1718804115>.
22. Son HF, Cho IJ, Joo S, Seo H, Sagong H-Y, Choi SY, Lee SY, Kim K-J. 2019. Rational protein engineering of thermo-stable PETase from *Ideonella sakaiensis* for highly efficient PET degradation. *ACS Catal* 9:3519–3526. <https://doi.org/10.1021/acscatal.9b00568>.
23. Cui Y, Chen Y, Liu X, Dong S, Tian Y, Qiao Y, Mitra R, Han J, Li C, Han X, Liu W, Chen Q, Wei W, Wang X, Du W, Tang S, Xiang H, Liu H, Liang Y, Houk KN, Wu B. 2021. Computational redesign of a PETase for plastic biodegradation under ambient condition by the GRAPE strategy. *ACS Catal* 11:1340–1350. <https://doi.org/10.1021/acscatal.0c05126>.
24. Bollinger A, Thies S, Knieps-Grünhagen E, Gertzen C, Kobus S, Höppner A, Ferrer M, Gohlke H, Smits SHJ, Jaeger K. 2020. A novel polyester hydrolase from the marine bacterium *Pseudomonas aestuans*—structural and functional insights. *Front Microbiol* 11:114. <https://doi.org/10.3389/fmicb.2020.00114>.
25. Danso D, Schmeisser C, Chow J, Zimmermann W, Wei R, Leggewie C, Li X, Hazen T, Streit WR. 2018. New insights into the function and global distribution of polyethylene terephthalate (PET)-degrading bacteria and enzymes in marine and terrestrial metagenomes. *Appl Environ Microbiol* 84:e02773-17. <https://doi.org/10.1128/AEM.02773-17>.
26. Gerday C, Aittaleb M, Arpigny JL, Baise E, Chessa JP, Garsoux G, Petrescu I, Feller G. 1997. Psychrophilic enzymes: a thermodynamic challenge. *Biochim Biophys Acta* 1342:119–131. [https://doi.org/10.1016/s0167-4838\(97\)00093-9](https://doi.org/10.1016/s0167-4838(97)00093-9).
27. Yakimov MM, Giuliano L, Gentile G, Crisafi E, Chernikova TN, Abraham WR, Lünsdorf H, Timmis KN, Golyshin PN. 2003. *Oleispira antarctica* gen. nov., sp. nov., a novel hydrocarbonoclastic marine bacterium isolated from Antarctic coastal sea water. *Int J Syst Evol Microbiol* 53:779–785. <https://doi.org/10.1099/ijs.0.02366-0>.
28. Feller G, Thiry M, Arpigny J-L, Mergeay M, Gerday C. 1990. Lipases from psychrotropic Antarctic bacteria. *FEMS Microbiol Lett* 66:239–243. <https://doi.org/10.1111/j.1574-6968.1990.tb04004.x>.
29. Kube M, Chernikova TN, Al-Ramahi Y, Beloqui A, Lopez-Cortez N, Guazzaroni M-E, Heipieper HJ, Klages S, Kotsyurbenko OR, Langer I, Nechitaylo TY, Lünsdorf H, Fernández M, Juárez S, Ciordia S, Singer A, Kagan O, Egorova O, Petit PA, Stogios P, Kim Y, Tchigvintsev A, Flick R, Denaro R, Genovese M, Albar JP, Reva ON, Martínez-Gomariz M, Tran H, Ferrer M, Savchenko A, Yakunin AF, Yakimov MM, Golyshina OV, Reinhardt R, Golyshin PN. 2013. Genome sequence and functional genomic analysis of the oil-degrading bacterium *Oleispira antarctica*. *Nat Commun* 4:2156. <https://doi.org/10.1038/ncomms3156>.
30. Schmidt J, Wei R, Oeser T, Belisário-Ferrari MR, Barth M, Then J, Zimmermann W. 2016. Effect of Tris, MOPS, and phosphate buffers on the hydrolysis of polyethylene terephthalate films by polyester hydrolases. *FEBS Open Bio* 6:919–927. <https://doi.org/10.1002/2211-5463.12097>.
31. Bartnikowski M, Dargaville TR, Ivanovski S, Huttmacher DW. 2019. Degradation mechanisms of polycaprolactone in the context of chemistry, geometry and environment. *Prog Polym Sci* 96:1–20. <https://doi.org/10.1016/j.progpolymsci.2019.05.004>.
32. Wei R, Oeser T, Then J, Kühn N, Barth M, Schmidt J, Zimmermann W. 2014. Functional characterization and structural modeling of synthetic polyester-degrading hydrolases from *Thermomonospora curvata*. *AMB Express* 4:44. <https://doi.org/10.1186/s13568-014-0044-9>.
33. Leaver-Fay A, Tyka M, Lewis SM, Lange OF, Thompson J, Jacak R, Kaufman K, Renfrew PD, Smith CA, Sheffler W, Davis IW, Cooper S, Triguille A, Mandell DJ, Richter F, Ban YEA, Fleishman SJ, Corn JE, Kim DE, Lyskov S, Berrondo M, Mentzer S, Popović Z, Havranek JJ, Karanicolas J, Das R, Meiler J, Kortemme T, Gray JJ, Kuhlman B, Baker D, Bradley P. 2011. Rosetta3: an object-oriented software suite for the simulation and design of macromolecules. *Methods Enzymol* 487:545–574. <https://doi.org/10.1016/b978-0-12-381270-4.00019-6>.
34. Kirley TL. 1989. Reduction and fluorescent labeling of cyst(e)ine-containing proteins for subsequent structural analyses. *Anal Biochem* 180:231–236. [https://doi.org/10.1016/0003-2697\(89\)90422-3](https://doi.org/10.1016/0003-2697(89)90422-3).
35. Alcamán-Arias ME, Fariás L, Verdugo J, Alarcón-Schumacher T, Díez B. 2018. Microbial activity during a coastal phytoplankton bloom on the Western Antarctic Peninsula in late summer. *FEMS Microbiol Lett* 365:fny090. <https://doi.org/10.1093/femsle/fny090>.
36. Bankevich A, Nurk S, Antipov D, Gurevich AA, Dvorkin M, Kulikov AS, Lesin VM, Nikolenko SI, Pham S, Pribelski AD, Pyshkin AV, Sirotkin AV, Vyahhi N, Tesler G, Alekseyev MA, Pevzner PA. 2012. SPAdes: a new genome assembly algorithm and its applications to single-cell sequencing. *J Comput Biol* 19:455–477. <https://doi.org/10.1089/cmb.2012.0021>.
37. Hyatt D, Chen G-L, LoCascio PF, Land ML, Larimer FW, Hauser LJ. 2010. Prodigal: prokaryotic gene recognition and translation initiation site identification. *BMC Bioinformatics* 11:119. <https://doi.org/10.1186/1471-2105-11-119>.
38. Zhang Z, Schäffer AA, Miller W, Madden TL, Lipman DJ, Koonin EV, Altschul SF. 1998. Protein sequence similarity searches using patterns as seeds. *Nucleic Acids Res* 26:3986–3990. <https://doi.org/10.1093/nar/26.17.3986>.
39. Almagro Armenteros JJ, Tsirigos KD, Sønderby CK, Petersen TN, Winther O, Brunak S, von Heijne G, Nielsen H. 2019. SignalP 5.0 improves signal peptide predictions using deep neural networks. *Nat Biotechnol* 37:420–423. <https://doi.org/10.1038/s41587-019-0036-z>.
40. Alarcón-Schumacher T, Guajardo-Leiva S, Antón J, Díez B. 2019. Elucidating viral communities during a phytoplankton bloom on the West Antarctic Peninsula. *Front Microbiol* 10:1014. <https://doi.org/10.3389/fmicb.2019.01014>.
41. Langmead B, Salzberg SL. 2012. Fast gapped-read alignment with Bowtie 2. *Nat Methods* 9:357–359. <https://doi.org/10.1038/nmeth.1923>.
42. Nikolaidis E, Dimopoulou P, Maslak V, Nikodinovic-Runic J, Topakas E. 2020. Discovery and biochemical characterization of a novel polyestherase for the degradation of synthetic plastics. *Chem Proc* 2:33.
43. Santiago M, Ramírez-Sarmiento CA, Zamora RA, Parra LP. 2016. Discovery, molecular mechanisms, and industrial applications of cold-active enzymes. *Front Microbiol* 7:1408. <https://doi.org/10.3389/fmicb.2016.01408>.
44. Wei R, Song C, Grasing D, Schneider T, Bielytskiy P, Böttcher D, Matysik J, Bornscheuer UT, Zimmermann W. 2019. Conformational fitting of a flexible oligomeric substrate does not explain the enzymatic PET degradation. *Nat Commun* 10:3–6. <https://doi.org/10.1038/s41467-019-13492-9>.
45. Dong X, Xing T, Chen G. 2020. Improving the anti-pilling performance of cellulose fiber blended knitted fabrics with 2,4,6-trichloropyrimidine treatment. *Coatings* 10:969–916. <https://doi.org/10.3390/coatings10100969>.
46. Meyer-Cifuentes IE, Werner J, Jehmlich N, Will SE, Neumann-Schaal M, Öztürk B. 2020. Synergistic biodegradation of aromatic-aliphatic copolyester plastic by a marine microbial consortium. *Nat Commun* 11:5790. <https://doi.org/10.1038/s41467-020-19583-2>.
47. Magrane M, Consortium U, UniProt Consortium. 2011. UniProt Knowledgebase: a hub of integrated protein data. *Database (Oxford)* 2011:bar009. <https://doi.org/10.1093/database/bar009>.
48. Ishida T, Kinoshita K. 2007. PrDOS: prediction of disordered protein regions from amino acid sequence. *Nucleic Acids Res* 35:W460–W464. <https://doi.org/10.1093/nar/gkm363>.
49. Bradford MM. 1976. A rapid and sensitive method for the quantitation of microgram quantities of protein utilizing the principle of protein-dye binding. *Anal Biochem* 72:248–254. <https://doi.org/10.1006/abio.1976.9999>.
50. Stainmesse S, Orecchioni AM, Nakache E, Puisieux F, Fessi H. 1995. Formation and stabilization of a biodegradable polymeric colloidal suspension of nanoparticles. *Colloid Polym Sci* 273:505–511. <https://doi.org/10.1007/BF00656896>.
51. Belisário-Ferrari MR, Wei R, Schneider T, Honak A, Zimmermann W. 2019. Fast turbidimetric assay for analyzing the enzymatic hydrolysis of polyethylene terephthalate model substrates. *J Biotechnol* 14:1800272. <https://doi.org/10.1002/biot.201800272>.
52. Wei R, Oeser T, Barth M, Weigl N, Lübs A, Schulz-Siegmund M, Hacker MC, Zimmermann W. 2014. Turbidimetric analysis of the enzymatic hydrolysis of polyethylene terephthalate nanoparticles. *J Mol Catal B Enzym* 103:72–78. <https://doi.org/10.1016/j.molcatb.2013.08.010>.
53. Palm GJ, Reisky L, Böttcher D, Müller H, Michels EAP, Walczak MC, Berndt L, Weiss MS, Bornscheuer UT, Weber G. 2019. Structure of the plastic-

- degrading *Ideonella sakaiensis* MHEase bound to a substrate. *Nat Commun* 10:1717. <https://doi.org/10.1038/s41467-019-09326-3>.
54. Berman HM, Westbrook J, Feng Z, Gilliland G, Bhat TN, Weissig H, Shindyalov IN, Bourne PE. 2000. The Protein Data Bank. *Nucleic Acids Res* 28:235–242. <https://doi.org/10.1093/nar/28.1.235>.
  55. Ribitsch D, Hromic A, Zitzenbacher S, Zartl B, Gamerith C, Pellis A, Jungbauer A, Łyskowski A, Steinkellner G, Gruber K, Tscheliessnig R, Herrero Acero E, Guebitz GM. 2017. Small cause, large effect: Structural characterization of cutinases from *Thermobifida cellulosilytica*. *Biotechnol Bioeng* 114:2481–2488. <https://doi.org/10.1002/bit.26372>.
  56. Roth C, Wei R, Oeser T, Then J, Föllner C, Zimmermann W, Sträter N. 2014. Structural and functional studies on a thermostable polyethylene terephthalate degrading hydrolase from *Thermobifida fusca*. *Appl Microbiol Biotechnol* 98:7815–7823. <https://doi.org/10.1007/s00253-014-5672-0>.
  57. Bender BJ, Cisneros A, Duran AM, Finn JA, Fu D, Lokits AD, Mueller BK, Sangha AK, Sauer MF, Sevy AM, Sliwoski G, Sheehan JH, DiMaio F, Meiler J, Moretti R. 2016. Protocols for molecular modeling with Rosetta3 and RosettaScripts. *Biochemistry* 55:4748–4763. <https://doi.org/10.1021/acs.biochem.6b00444>.
  58. Lüthy R, Bowie JU, Eisenberg D. 1992. Assessment of protein models with three-dimensional profiles. *Nature* 356:83–85. <https://doi.org/10.1038/356083a0>.
  59. Pontius J, Richelle J, Wodak SJ. 1996. Deviations from standard atomic volumes as a quality measure for protein crystal structures. *J Mol Biol* 264: 121–136. <https://doi.org/10.1006/jmbi.1996.0628>.
  60. Laskowski RA, MacArthur MW, Moss DS, Thornton JM. 1993. PROCHECK: a program to check the stereochemical quality of protein structures. *J Appl Crystallogr* 26:283–291. <https://doi.org/10.1107/S0021889892009944>.
  61. Hooft RWW, Vriend G, Sander C, Abola EE. 1996. Errors in protein structures. *Nature* 381:272–272. <https://doi.org/10.1038/381272a0>.
  62. Song Y, Dimairo F, Wang RYR, Kim D, Miles C, Brunette T, Thompson J, Baker D. 2013. High-resolution comparative modeling with RosettaCM. *Structure* 21:1735–1742. <https://doi.org/10.1016/j.str.2013.08.005>.
  63. Maier JA, Martinez C, Kasavajhala K, Wickstrom L, Hauser KE, Simmerling C. 2015. ff14SB: improving the accuracy of protein side chain and backbone parameters from ff99SB. *J Chem Theory Comput* 11:3696–3713. <https://doi.org/10.1021/acs.jctc.5b00255>.
  64. Anandakrishnan R, Aguilar B, Onufriev AV. 2012. H++ 3.0: automating pK prediction and the preparation of biomolecular structures for atomistic molecular modeling and simulations. *Nucleic Acids Res* 40:W537–W541. <https://doi.org/10.1093/nar/gks375>.
  65. Ryckaert JP, Ciccotti G, Berendsen HJC. 1977. Numerical integration of the cartesian equations of motion of a system with constraints: molecular dynamics of n-alkanes. *J Comput Phys* 23:327–341. [https://doi.org/10.1016/0021-9991\(77\)90098-5](https://doi.org/10.1016/0021-9991(77)90098-5).
  66. Darden T, York D, Pedersen L. 1993. Particle mesh Ewald: an  $N^2 \log(N)$  method for Ewald sums in large systems. *J Chem Phys* 98:10089–10092. <https://doi.org/10.1063/1.464397>.
  67. Roe DR, Cheatham TE. 2013. PTRAJ and CPPTRAJ: software for processing and analysis of molecular dynamics trajectory data. *J Chem Theory Comput* 9:3084–3095. <https://doi.org/10.1021/ct400341p>.
  68. Bengtsson-Palme J, Hartmann M, Eriksson KM, Pal C, Thorell K, Larsson DGJ, Nilsson RH. 2015. metaxa2: improved identification and taxonomic classification of small and large subunit rRNA in metagenomic data. *Mol Ecol Resour* 15:1403–1414. <https://doi.org/10.1111/1755-0998.12399>.